

Geophysical Research Letters[®]



RESEARCH LETTER

10.1029/2023GL103672

GEORGIA: A Graph Neural Network Based EmulatOR for Glacial Isostatic Adjustment

Yucheng Lin¹ , Pippa L. Whitehouse¹ , Andrew P. Valentine^{2,3} , and Sarah A. Woodroffe¹ 

¹Department of Geography, Durham University, Durham, UK, ²Department of Earth Sciences, Durham University, Durham, UK, ³Research School of Earth Sciences, The Australian National University, Acton, ACT, Australia

Key Points:

- The first attempt to build a deep-learning based Glacial isostatic adjustment (GIA) emulator that can accurately predict global sea-level change based on a given ice model
- This emulator (GEORGIA) can predict global sea-level change history within 0.5 s with minor emulation error
- This GIA emulator along with two illustrative applications are available for use by the wider sea-level community

Supporting Information:

Supporting Information may be found in the online version of this article.

Correspondence to:

Y. Lin,
yucheng.lin@durham.ac.uk

Citation:

Lin, Y., Whitehouse, P. L., Valentine, A. P., & Woodroffe, S. A. (2023). GEORGIA: A graph neural network based EmulatOR for glacial isostatic adjustment. *Geophysical Research Letters*, 50, e2023GL103672. <https://doi.org/10.1029/2023GL103672>

Received 13 MAR 2023

Accepted 9 AUG 2023

Author Contributions:

Conceptualization: Yucheng Lin, Pippa L. Whitehouse, Andrew P. Valentine
Data curation: Yucheng Lin
Formal analysis: Yucheng Lin
Investigation: Yucheng Lin, Pippa L. Whitehouse, Andrew P. Valentine
Methodology: Yucheng Lin, Pippa L. Whitehouse, Andrew P. Valentine, Sarah A. Woodroffe
Supervision: Pippa L. Whitehouse, Andrew P. Valentine, Sarah A. Woodroffe

© 2023. The Authors. Geophysical Research Letters published by Wiley Periodicals LLC on behalf of American Geophysical Union.

This is an open access article under the terms of the [Creative Commons Attribution License](https://creativecommons.org/licenses/by/4.0/), which permits use, distribution and reproduction in any medium, provided the original work is properly cited.

Abstract Glacial isostatic adjustment (GIA) modeling is not only useful for understanding past relative sea-level change but also for projecting future sea-level change due to ongoing land deformation. However, GIA model predictions are subject to a range of uncertainties, most notably due to uncertainty in the input ice history. An effective way to reduce this uncertainty is to perform data-model comparisons over a large ensemble of possible ice histories, but this is often impossible due to computational limitations. Here we address this problem by building a deep-learning-based GIA emulator that can mimic the behavior of a physics-based GIA model while being computationally cheap to evaluate. Assuming a single 1-D Earth rheology, our emulator shows 0.54 m mean absolute error on 150 out-of-sample testing data with <0.5 s emulation time. Using this emulator, two illustrative applications related to the calculation of barystatic sea level are provided for use by the sea-level community.

Plain Language Summary Piecing together the history of ice sheet change during past glacial cycles is not only important for understanding past sea-level change but also for predicting how ongoing glacial rebound contributes to future sea-level change. Traditionally, a physics-based “sea-level model” is used to predict the sea-level change associated with a particular reconstruction of past ice sheet change and compare the results with geological records of past sea level. However, a fundamental limitation of this approach is the need to compute sea-level change for a large number of plausible ice histories, which is often prohibited by the computational resources required to repeatedly solve the complex physical equations. In this paper, we describe a machine-learning-based statistical model that can mimic the behavior of a physics-based sea-level model. This statistical model is computationally cheap and we demonstrate that it is able to accurately predict global sea-level change for a suite of 150 “unseen” ice histories. Our statistical model predicts sea-level change 100–1,000 times faster than a physics-based model, making it an ideal tool for investigating and improving our understanding of global ice sheet change.

1. Introduction

During Quaternary glacial cycles, water-mass redistribution related to the waxing and waning of ice sheets altered global mean sea-level by as much as ~130 m. The spatially variable response of the solid Earth, oceans and global gravitational field to that change in water mass is known as glacial isostatic adjustment (GIA), a process which causes local relative sea level (RSL; distance between the sea surface and the solid Earth) to differ substantially from global mean sea level. GIA models that describe RSL change (Farrell & Clark, 1976; Whitehouse, 2018) have been widely used to investigate past (Lambeck et al., 2014; Lin et al., 2021), present (Frederikse et al., 2020; Hay et al., 2015) and future (Caron et al., 2018; Love et al., 2016) sea-level change problems. Within GIA modeling, a key parametric uncertainty relates to poorly constrained ice histories, which not only reduces our confidence in understanding past sea-level change but also limits our ability to robustly project future sea-level variation due to the ongoing GIA effects associated with past glacial cycles.

A commonly used approach to reduce ice history uncertainty involves performing data-model comparisons with geological data that relate to ice-sheet history: either directly for example, geomorphological evidence of past glaciation, or indirectly such as RSL records. Due to the sparse and noisy nature of geological records, a range of plausible ice-sheet histories may be compatible with the observations, and a robust study often requires testing a large number of these to explore what can be and cannot be constrained (Briggs et al., 2014; Tarasov et al., 2012). However, it is computationally expensive to solve the complex physical equations required to perform data-model comparison. An effective way to mitigate this difficulty is to build a statistical model that mimics the behavior of

Visualization: Yucheng Lin

Writing – original draft: Yucheng Lin

Writing – review & editing: Pippa L.

Whitehouse, Andrew P. Valentine, Sarah
A. Woodroffe

the physics-based simulator but is computationally cheap to run (Reichstein et al., 2019). Rather than solving the physical equations exactly, these “statistical emulators” learn how the system behaves based on a (comparatively) small set of examples, and use this to predict what the simulation would output in other scenarios.

The concept of emulation (also known as “surrogate modeling”) is not particularly new (Sacks et al., 1989), but recent advances in machine learning have greatly expanded its scope and application (Reichstein et al., 2019). Recent studies have built statistical emulators to quantify the impact of basal melt on dynamic ice-sheet model behavior (Berdahl et al., 2021) and to investigate how different CO₂ emission scenarios affect ice-sheet model estimates for future sea-level rise (Edwards et al., 2021). For sea-level research, although Tarasov and Peltier (2005) and Tarasov et al. (2012) created a neural-network-based emulator that can predict RSL chronologies based on a set of glacial systems model parameters, there is currently no end-to-end GIA emulator that can predict global RSL variation history based on arbitrary ice models. In this study, we document a proof-of-concept attempt to build an end-to-end Graph neural network based EmulatOR for GIA (GEORGIA) that can be used to rigorously explore global ice history uncertainty.

2. Methodology

Our goal is to build a statistical emulator that can predict global RSL variation based on a given global ice history from 25 ka BP to present. This can be treated as a supervised regression problem that maps the statistical relationship between input and output based on example input-output pairs generated by a physics-based GIA model. Below, we describe the example data generation, data pre-processing, and the methods used to build and validate our emulator.

2.1. Training Data

To provide example input-output pairs for training our emulator, we use a physics-based GIA model to calculate global RSL variation based on a collection of ice sheet reconstructions. The physical model we use is a gravitationally self-consistent GIA model that accounts for shoreline migration and Earth rotational feedback (Kendall et al., 2005; Milne & Mitrovica, 1996; Mitrovica et al., 2005). The solid Earth is represented by a spherically symmetric Maxwell body consisting of an elastic lithosphere, and an upper and lower mantle extending to 670 km, and from 670 km to the core-mantle boundary, respectively. The GIA model calculates RSL change, caused by land deformation and the geoid response to ice-water mass redistribution, by solving the sea-level equation (Mitrovica et al., 2005) using a spherical harmonic truncation of degree and order 256. The elastic and density structure of the Earth model is derived from the preliminary reference Earth model (Dziewonski & Anderson, 1981). Because the major focus of this study is to thoroughly sample ice history uncertainty, we do not incorporate Earth model parameter variation within the input data for our emulator. Instead, we adopt one specific Earth rheology that has a lithospheric thickness of 71 km and an upper and lower mantle viscosity of 0.3 and 70×10^{20} Pa s respectively (the “low-viscosity” Earth model scenario from Lambeck et al. (2014)).

One key task when building a GIA emulator is to generate a training database which evenly covers a wide range of possible deglaciation trajectories. We achieve this by collecting a wide range of ice history models for four different regions: North America (including Greenland), Eurasia, Antarctica, and all other regions with mountain glaciers (including Patagonia), and sampling the spatio-temporal variability between different reconstructions. In total, we use four global ice models that predict ice-sheet evolution in the four regions (Gowan et al., 2021; Lambeck et al., 2014; Peltier, 2004; Peltier et al., 2015), along with four North American (Gowan et al., 2016; Han et al., 2021; Roy & Peltier, 2018; Tarasov & Peltier, 2003; Tarasov et al., 2012), four Eurasian (Abe-Ouchi et al., 2013; Clark et al., 2021; Han et al., 2021; Patton et al., 2016, 2017; Tarasov et al., 2014) and three Antarctic (Argus et al., 2014; Briggs et al., 2014; Whitehouse, Bentley, & Le Brocq, 2012; Whitehouse, Bentley, Milne, et al., 2012) ice models. Because these ice models are reconstructed based on different principles (e.g., thermo-mechanical ice modeling, GIA modeling, and the interpolation of glacial geomorphological data), they provide good coverage of possible ice-sheet deglaciation uncertainty. Detailed information about each ice model is given in Table S1 of the Supporting Information S1. We resample all the ice sheet reconstructions into a standardized format with 26 time slices (from 25 to 0 ka at 1 ka intervals) and spatial coverage corresponding to 256° spherical harmonic truncation, using linear interpolation as necessary. Because a GIA model is forced by ice thickness change rather than total ice thickness, we express all ice models in terms of ice thickness relative to present.

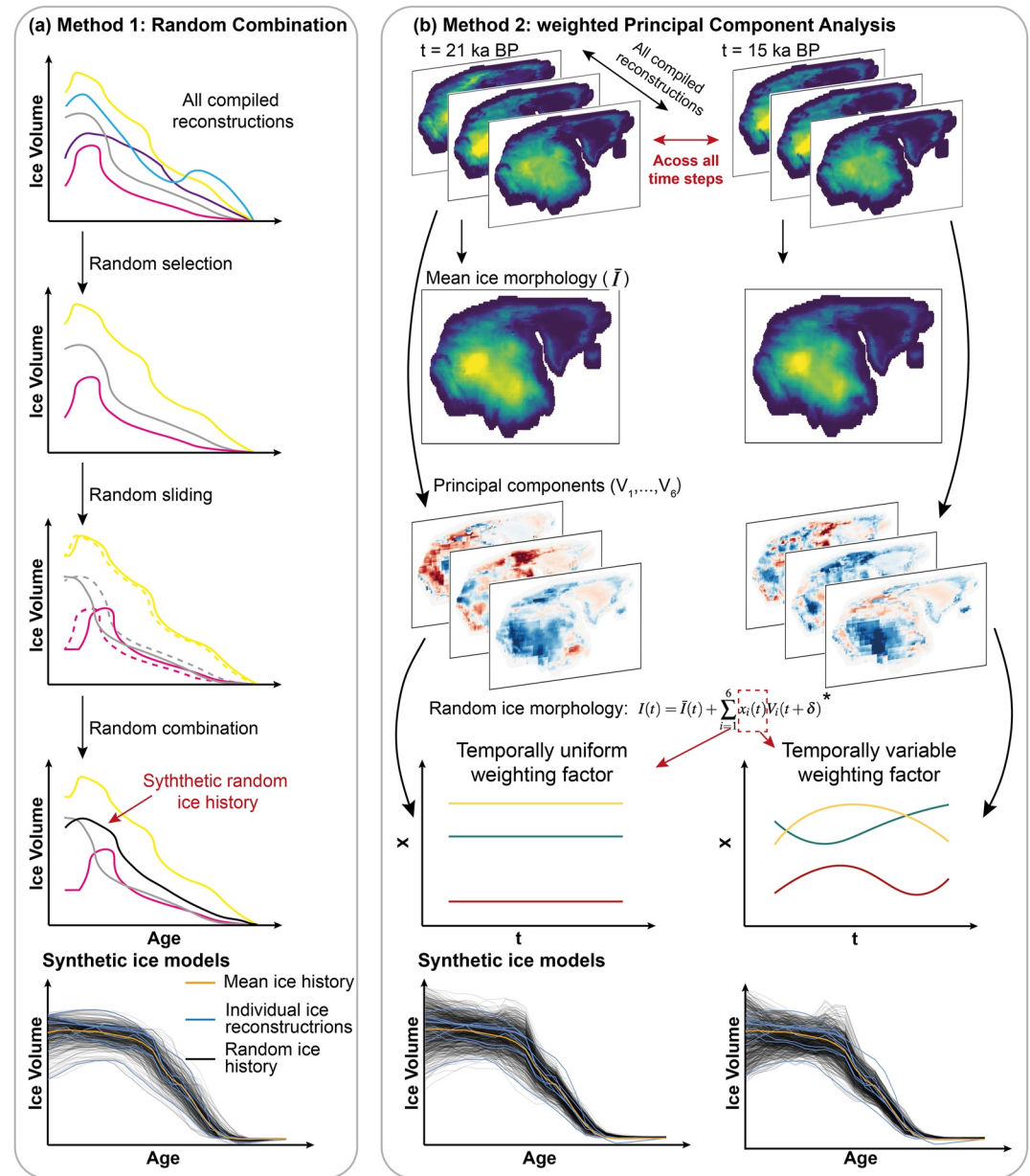


Figure 1. Illustration of the methods used to generate random synthetic ice histories from previous ice sheet reconstructions. (a) Random combination method, which consists of three randomized sampling procedures that reflect temporal (random selection and sliding) and spatial uncertainty (random selection and combination) in the underlying ice sheet reconstructions. (b) Weighted Principal Component Analysis method, which is implemented by calculating the mean ice sheet morphology and principal components of all time slices. From these, random ice sheet morphologies are generated via linear combination of the randomized principal components using two different temporal treatments of the random factor $x_i(t)$, which is illustrated by the equation with an asterisk. A detailed description of this equation can be found in Text S2 of the Supporting Information S1. The resulting synthetic random ice histories are shown in the bottom panel. All examples shown here are for the North American Ice Sheet, but the same approach was used to sample the Antarctic and Eurasian Ice Sheets, as well as mountain glaciers, to create a synthetic global ice history.

Using these standardized ice sheet reconstructions as building blocks, we generate a suite of randomized, synthetic ice histories that span the range of plausibility. We employ two main methods to systematically sample the spatio-temporal variability across different reconstructions: random combination and weighted principal component analysis (wPCA). The random combination method samples the variability within the range bounded by previous reconstructions (Figure 1a), while the wPCA approach samples out-of-boundary variability, with two

different strategies employed to account for long-term (e.g., grounded ice volume at the Last Glacial Maximum, Simms et al., 2019) and short-term (e.g., Meltwater Pulse 1A; Deschamps et al., 2012; Lin et al., 2021) temporal variability (Figure 1b). We provide a brief summary of these approaches here, with a detailed description given in Texts S1 and S2 of the Supporting Information S1. The random combination method creates 500 synthetic ice histories by linearly combining different ice models into a new model. We randomly select 2–6 ice models for each region (i.e., random selection in Figure 1), and randomly translate each in time (younger or older) in order to sample the temporal uncertainty. The new ice model is calculated to be the weighted average of the selected ice models, with the details determined using a set of random weighting factors. The second approach uses wPCA to extract important ice morphological patterns (i.e., principal components; PCs) from different ice models. A weighting scheme is applied to account for the spherical geometry of the Earth, which means that grid cells at different latitudes cover different areas. Using the extracted PCs, 1,000 synthetic ice histories (500 for each strategy to temporal uncertainty) are generated by adding a random linear combination of the PCs to the mean ice history (Figure 1b; details in Text S2 of the Supporting Information S1).

After obtaining 1,500 synthetic ice histories for each region, we create global ice models by randomly selecting ice models for each region, with the result that one global ice model may contain regional ice histories generated by several different statistical methods. In total, we create 1,500 synthetic global ice histories. For each we then simulate global RSL history from 25 ka to present, as described above. Because we express the input in terms of ice thickness relative to present, the modern ice thickness layer is a spatially uniform layer with all zero values, which contains no information. Therefore, we replace this layer with modern topography, which is important for calculating the continental levering and ocean siphoning processes (Mitrovica & Milne, 2002). Before being used to train a GIA emulator, we normalize all input and output data to ensure zero mean and unit standard deviation (more information in Text S3 of the Supporting Information S1). The 1,500 normalized input-output pairs are divided into training (80%), validation (10%) and testing (10%) sets.

2.2. Statistical Emulator

Using this training set, we now wish to build an emulator that can map ice history into RSL change. This is a typical machine learning problem, for which a convolutional neural network is commonly used. However, classical convolutional neural network algorithms are designed to perform convolution and pooling operations within Euclidean space, which is not appropriate when representing geographical data such as ice or RSL history on a spherical Earth. Therefore, we use a graph-based spherical convolutional neural network (SCNN) algorithm that correctly implements convolution and pooling operations on data within a spherical manifold. We employ a Hierarchical Equal Area isoLatitude Pixelization (Healpix) scheme to build this spherical manifold, which produces a subdivision of a spherical surface where every pixel covers the same surface area (Gorski et al., 2005). This is an ideal property for emulating GIA processes because it ensures that input ice thickness is proportional to the ice load applied to each grid cell. Furthermore, the SCNN algorithms used in this study use a graph filter that extracts information from nearby grid cells in a way that only depends on the distance between the grid centers, not on the direction. This ensures that information is rotationally equivariant. In other words, rotating the input ice history will result in an equivariant output RSL prediction. Rotational equivariance is desirable because it can significantly reduce the data sampling complexity. Underpinning these SCNN algorithms is a 3-layer U-Net (Ronneberger et al., 2015), a neural network architecture that is widely used in regression and image segmentation problems (Lai et al., 2020; Yao et al., 2018)—see Text S4 in Supporting Information S1 for more details. For this study, we adopt the SCNN algorithms from the *DeepSphere* package (Defferrard et al., 2019, 2020), which has been successfully used in cosmological and weather prediction applications (Perraudin et al., 2019).

The emulator structure is governed by various hyperparameters, whose values influence the final emulation performance. Here we provide information on some key hyperparameters used in this study; a full list of the hyperparameters along with selection criteria are given in Text S5 of the Supporting Information S1. A hyperparameter that should be noted is the Healpix sampling resolution. To achieve relatively fast emulation, we use a 16° Healpix sampling resolution ($n = 3,072$), corresponding to $\sim 3.66^\circ$ spatial coverage. All standardized input and output fields are interpolated onto 16° Healpix grids. Another essential hyperparameter for SCNNs is graph filter size, which determines the number of nearest-neighborhoods included in each convolution process (i.e., spatial scale length). This is important for GIA problems because the solid Earth deformation signal tends to be long wavelength. For example, the peripheral bulge formed in response to loading of the North American Ice Sheet

can extend over 3,000 km, to places like Barbados. In this study, we use a graph filter size of 60, corresponding to $\sim 1,780$ km radius.

We use a mean square error (MSE) loss function to quantify the misfit between predictions and observations and iteratively update model parameters by backpropagation (Goodfellow et al., 2016). Because the MSE loss function focuses on the misfit of each single grid point, we include two extra metrics to assess the overall quality of the emulation results: peak signal-to-noise ratio (PSNR, Korhonen & You, 2012) and structural similarity index measure (SSIM, Brunet et al., 2011). Both of these metrics are widely used to measure the quality of image and video compression (Huynh-Thu & Ghanbari, 2008; Wang & Bovik, 2009), with formal definitions given in Text S6 of the Supporting Information S1. A high PSNR value indicates low noise level, and vice versa, while the SSIM provides a similarity metric between 0 and 1 where a higher value indicates better emulation quality. Note that the SSIM is not directly correlated with either MSE or PSNR, and so can provide an independent assessment of output quality (Hore & Ziou, 2010). We also evaluate model performance by calculating the mean absolute error (MAE). This metric is arguably more directly interpretable than the root-mean-square error, which was used during emulator training for its mathematical convenience. To produce predictive uncertainty estimates, we adopt an ensemble learning approach, which is proved to be an efficient tool for estimating neural network based emulator uncertainty (Lakshminarayanan et al., 2017). The approach involves training an ensemble of 30 alternative SCNNs. The SCNNs all have the same model structure but they are initialized using different model weights and they use different training examples. The 1,200 training examples are constructed by randomly sampling our training and validation sets (the testing set remains unseen for all SCNNs). The variance between the 30 SCNNs represents GEORGIA's predictive uncertainty.

Finally, to assess the value of the SCNN model, and explore whether it is able to capture significant internal relationships between inputs and outputs, we also create a basic kernel model. When given previously unseen inputs, this model simply finds the five most similar inputs from within the training set, and averages their known outputs. The misfit of this approach serves as a baseline for assessing the performance of the SCNN-based emulator.

3. Results and Discussions

3.1. Emulator Performance

Using the trained SCNN-based emulator, which will be referred to as GEORGIA, we predict RSL variation results for 150 unseen testing examples. GEORGIA out-performs the kernel-based method on all evaluation metrics. Specifically, GEORGIA achieves an order of magnitude lower MSE (0.946 vs. 29.53 m²) and MAE (0.54 vs. 5.84 m) along with distinctly higher PSNR (61.11 vs. 46.18) and SSIM (0.9995 vs. 0.9864) values. This indicates that the SCNN-based algorithm is able to capture the complex correlation between ice history and GIA-induced RSL history better than the baseline approach of finding similar training set pairs. The low MSE and MAE values, and the high PSNR and SSIM values, suggest a high-level of similarity between the RSL predictions generated by the emulator and the physical-based model. The 0.54 m MAE emulation error is also smaller than 87.8% of the 2σ RSL reconstruction uncertainties in a comprehensive sea-level database (Hibbert et al., 2018), suggesting a sufficient emulation accuracy.

The spatial and temporal distributions of emulation error between the physical and statistical models are shown in Figure 2. The emulation MAE is strongly heterogeneous in space (Figure 2a), with near-field regions showing large errors of up to 4 m, while errors in far-field regions (i.e., far from previous ice-sheet margins) are mostly below 0.5 m. This spatial heterogeneity reflects the spatial variability in the training set (Figure S1d in Supporting Information S1), where near- and far-field RSL standard deviations can reach up to 500 and 25 m, respectively, indicating that the average emulation error is 1%–2% of the training variability.

Temporally, emulation MAE is generally higher during the early stages of deglaciation (Figure 2b), when RSL is significantly different from present-day values (Figure 2b). Emulation MAE peaks between 20 and 10 ka BP due to the rapid unloading of the major ice sheets, and it decreases during the Holocene as global mean sea-level gradually approaches modern levels. Figures 2d–2f show physics-based RSL predictions along with the emulation error at three typical near-, intermediate- and far-field sea-level sites. It is clear that although RSL predictions differ significantly between these sites, the temporal distributions of the emulation error follow an identical near-stationary trend, with larger emulation error occurring before the Holocene, similar to the global average

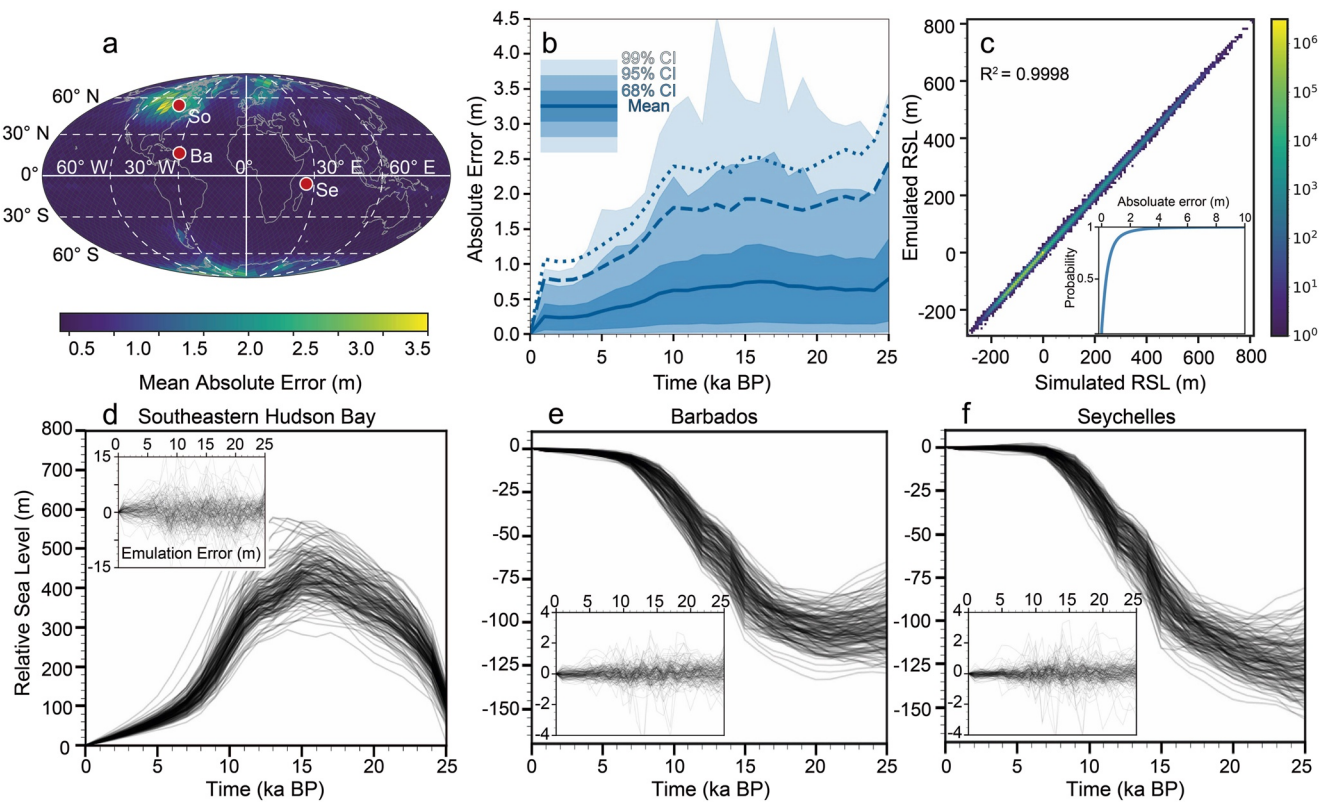


Figure 2. Emulator performance for the 150-member out-of-sample testing set. (a) Temporally averaged spatial distribution of emulation error, locations here refer to typical near-, intermediate- and far-field sites: (So) Southeastern Hudson Bay; (Ba) Barbados and (Se) Seychelles. (b) Mean and confidence intervals of spatially averaged temporal variation of the emulation error and predictive uncertainty, where colored areas indicate the emulation error confidence interval and dashed/dotted lines denote the upper range of 95/99% confidence interval of predictive uncertainty produced by GEORGIA; CI = confidence interval. (c) 2-D histogram comparing the ground truth and emulator predictions. R^2 denotes the coefficient of determination. The subplot shows the cumulative probability of the absolute error. (d–f) RSL predictions generated using the physics-based Glacial isostatic adjustment model for the 150-member test set, with emulation errors and time shown on the y and x axes in the subplots, at Southeastern Hudson Bay, Barbados and Seychelles, respectively.

pattern shown in Figure 2b. Considering this near-stationary and white-noise-like error distribution, we suggest that GEORGIA is able to capture the vast majority of correlation between ice history and the global RSL field.

Figure 2c provides an overall comparison between the physics- and statistical-based RSL predictions. It is clear that GEORGIA can well approximate the physics-based GIA model with a 0.9998 coefficient of determination (R^2) and no systematic error. 95.7% of the emulation results have a MAE of less than 2 m. In far-field regions, over 99% of the emulation results have a MAE of <2 m while 95% have a MAE of <1 m.

To assess the performance of GEORGIA's predictive uncertainty estimates, we compare them with emulation errors on unseen testing examples (Figure S4 in Supporting Information S1). The 3σ predictive uncertainties are mostly larger than the emulation errors with 99% of emulation predictive intervals (i.e., $\pm 3\sigma$) being able to encompass 94.5% of ground truth values. GEORGIA's predictive uncertainties also agree well with the temporal trend of emulation errors (Figure 2b). These observations suggest our uncertainty estimates are robust. However, for some extreme cases (e.g., the 97.5%–99.5% percentile of the emulation error in Figure 2b), GEORGIA's predictive uncertainties may slightly underestimate the emulation errors. Therefore, we show the 97.5% percentile of the emulation errors across the 150-member testing set at 9 different time steps (Figure S5 in Supporting Information S1) as a conservative estimate on emulation uncertainty, which can reach up to 14/3.5 m in the near/far field, corresponding to 5%–8% of the training variability.

Although GEORGIA contains ~33.8 million trainable parameters, it only takes 3.7 s to emulate RSL change through the last deglaciation on a Central Processing Unit (Intel® Core™ i9 14 Core Processor). The computation time decreases to 0.25 s when using a Graphics Processing Unit (8GB NVIDIA GEFORCE RTX 3070 Ti). This is 100–1,000 times faster than the computation time of our physical forward GIA model (see Section 2.1),

which takes 6 min to run three iterations (necessary to initialize palaeo topography), and where each iteration comprises 26 time steps at 256° spherical harmonic resolution. Considering the good emulation accuracy above, this emulator allows us to perform 100–1,000 times more simulations within a given computational budget—potentially making it feasible to employ a range of ensemble-based techniques for parameter estimation and uncertainty quantification.

3.2. GEORGIA Generalizability

A key question for any statistical emulator is generalizability: how does the emulator perform for arbitrary unseen inputs? For neural network based emulators, previous studies suggest that although they perform well in interpolation problems (GEORGIA performs well for unseen ice histories that are taken from a similar distribution to our training set, see Section 3.1 and further examples in Text S7 of the Supporting Information S1), they cannot meaningfully extrapolate non-linear functions (Goodfellow et al., 2016; Xu et al., 2020). In other words, while GEORGIA is effective for ice histories that are similar to those in our training set, GEORGIA may produce meaningless output if an ice sheet reconstruction has been generated using an approach or philosophy that is very different to the approach used to generate the ice history models included in our training set. This drawback means that in order to emulate a specific GIA problem, a well-designed training set is a prerequisite. Although our training set covers a wide range of possible ice histories by thoroughly sampling the spatio-temporal variability of previous ice-sheet reconstructions, this cross-reconstruction variability cannot describe the ice thickness uncertainty associated with poor knowledge of ice-sheet dynamical processes (e.g., large uncertainty in ice stream areas, Albrecht et al., 2020; Pittard et al., 2022; Tarasov et al., 2012) and ice margin chronology (Dalton et al., 2020). Therefore, incorporating more modeling results from physically consistent ice sheet models that are constrained by empirical geomorphological evidence will be an important forward step to further improve the generalization of GEORGIA.

3.3. Emulator Applications

Using GEORGIA, global RSL variation from 25 ka BP to present can be rapidly emulated using any ice history that is similar to our training set. Because our training set provides good coverage of possible deglaciation scenarios identified in previous studies, GEORGIA can be used as a substitute for a physics-based GIA model in many applications. Additionally, benefitting from a modern machine learning framework, GEORGIA can be used by other researchers with minimum requirements for programming experience or computational resources. Here, we provide two example GEORGIA applications, namely; (a) calculating the ice-sheet contribution to global Barystatic sea level (BSL); and (b) mapping BSL in space and time.

3.3.1. Barystatic Sea Level Calculator

BSL describes the uniform shift of the global ocean surface due to ice-ocean mass exchange in the absence of gravitational effects and Earth deformation. It is a direct measure of global grounded ice volume change through time, and hence it is important for calibrating isotopic proxies and constraining ice-sheet variation history (Waelbroeck et al., 2002). However, for palaeo ice-sheet modeling studies, there is no straightforward way to calculate the ice-sheet contribution to global BSL without running a GIA model, due to the complexities associated with changes in global ocean area and topography (which impacts the grounded-floating ice transition). As a result, numerous studies (e.g., Gomez et al., 2020; Patton et al., 2017) only present their ice modeling results in terms of ice volume or an ice volume equivalent sea-level contribution (i.e., ice volume divided by modern ocean area). Based on our physics-based GIA modeling results, this latter approach overestimates the ice sheet contribution to barystatic sea-level at 21 ka BP by 3.34 m (0.8–4.3 m depending on the adopted ice history), which is a non-negligible signal to consider.

Using GEORGIA, we provide a global BSL calculator that accounts for shoreline migration and the impact of solid Earth deformation on ice flotation (with detailed theory given in Text S8 of the Supporting Information S1). To test the accuracy of this GEORGIA-based BSL calculator, we compare its predictions to 150 examples of deglacial BSL history obtained using the physics-based model (i.e., those comprising the testing set). The results show emulation error (MAE) of 0.04 m. Thus, GEORGIA is a suitable tool to rapidly estimate the ice-sheet contribution to global BSL change, for example, as predicted by ice dynamic or general circulation models.

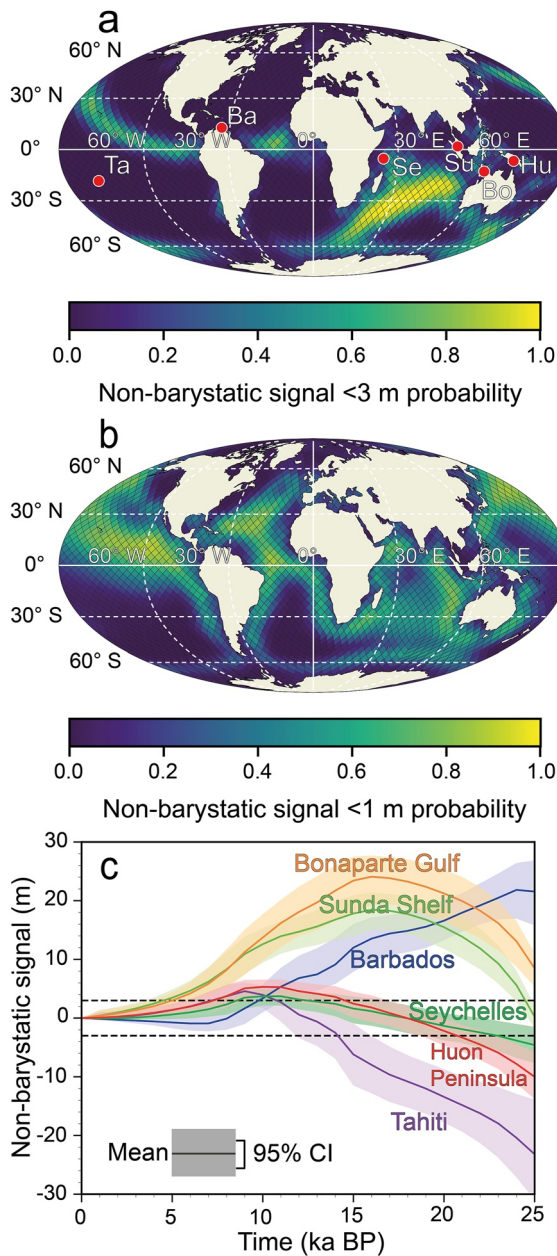


Figure 3. Barystatic sea-level maps based on 10,000 emulation results. (a) Probability that local RSL lies within 3 m of the barystatic value at 21 ka BP. (b) Probability that local RSL lies within 1 m of the barystatic value at 6 ka BP. (c) Temporal variation of the non-barystatic signal at six different sea-level sites. Note the confidence intervals shown here only reflect the uncertainty associated with combining 10,000 different ice histories with one Earth rheology. The non-barystatic signal indicates the difference between GIA-induced RSL change and Barystatic sea level without considering any steric effects. The area between the two black dashed lines represents the region where the non-barystatic signal is smaller than 3 m. Locations in (a) refer to (from west to east): Tahiti (Ta), Barbados (Ba), Seychelles (Se), Sunda Shelf (Su), Bonaparte Gulf (Bo) and Huon Peninsula (Hu).

3.3.2. Barystatic Sea Level Map

A barystatic sea-level map identifies locations and times where local RSL approximates global BSL. Such sites are targeted by sea-level scientists to provide a close constraint on global ice volume. Because of spatially and temporally variable GIA-related perturbations to the gravity field and solid Earth surface (i.e., the non-barystatic signal), producing a BSL map requires robust estimates of the non-barystatic contributions to RSL. The detailed theory for calculating a BSL map was described in Milne and Mitrovica (2008) where they conclude that ideal locations to reconstruct palaeo BSL are where local RSL: (a) is relatively insensitive to plausible ranges in GIA model parameters (i.e., global ice history and solid Earth rheology); (b) closely approximates the barystatic value. Milne and Mitrovica (2008) provide a series of BSL maps at different time slices, based on GIA modeling results that use two ice histories (Bassett et al., 2005; Peltier, 2004), each paired with 162 plausible sets of Earth parameters. These maps have been used by the field community to target locations that approximate BSL during different parts of the deglacial period (e.g., Sefton, 2020; Woodroffe et al., 2015).

A major limitation of Milne and Mitrovica (2008) is that they only sample two ice models, and hence they are not able to thoroughly quantify the impact of ice history uncertainty on the resulting BSL estimates. Because GEORGIA has high computational efficiency while remaining sufficiently accurate for many applications (Section 3.1), it is an ideal tool for testing the sensitivity of the BSL map to a large ensemble of ice histories. To produce a BSL map that represents ice history uncertainty, we emulate the global non-barystatic signal (i.e., RSL—BSL, neglecting any steric effects) for 10,000 randomly generated ice histories using the same methods introduced in Section 2.1. Based on these emulation results, we calculate the probability that global RSL lies within 3 and 1 m of the barystatic value at 21 and 6 ka BP respectively (Figure 3).

Because uncertainty in the results of Milne and Mitrovica (2008, see their Figures 6 and 7) largely reflects the uncertainty associated with radial mantle viscosity structure, combining their results with ours enables us to identify regions where, although RSL approximates the global BSL value with minimal sensitivity to the choice of radially varying Earth model, it is sensitive to the choice of ice history (e.g., offshore regions near eastern Australian at 21 ka BP). After excluding such regions, we conclude that the southern Indian Ocean and southern Tasman Sea (close to south-western New Zealand) are ideal regions to reconstruct global BSL at 21 ka BP because it is highly likely that the non-barystatic signal here will be lower than 3 m, and predictions are insensitive to the Earth model choice (Milne & Mitrovica, 2008). Although there is also a low non-barystatic signal shown in the mid-northern Pacific and mid Atlantic regions, these sites are not suitable for reconstructing global BSL because RSL is highly sensitive to the choice of Earth rheology (Milne & Mitrovica, 2008). For the mid-Holocene, our map shows a broadly similar pattern to Milne and Mitrovica (2008), where optimal regions are the western and eastern Indian Ocean, the mid-northern Pacific Ocean and the mid-southern Atlantic Ocean. Meanwhile, agreeing with the results from Milne and Mitrovica (2008), the mid-southern Atlantic is not an ideal region for mapping mid-Holocene BSL.

In Figure 3c, we show the impact of ice history uncertainty on the temporal evolution of the non-barystatic signal at six locations that are commonly used in sea-level studies (e.g., Lin et al., 2023; Webster et al., 2018; Woodroffe et al., 2015). Our results show that variations in the spatial and temporal distribution of the global ice sheets have a major effect on the magnitude of the non-barystatic signal, and a minor effect on the overall trend—the latter depends more on the Earth rheology, which we do not vary in this experiment. Regarding the six selected sea-level sites, as suggested in Milne and Mitrovica (2008), we confirm that the Seychelles is a particularly good site to map global BSL history because it has a low uncertainty, minor non-barystatic signal throughout the last deglaciation (Figure 3c). Although the Huon Peninsula is also predicted to have a small non-barystatic signal, and the uncertainty associated with ice history is small, this site is highly sensitive to the choice of Earth rheology (Milne & Mitrovica, 2008). In general, similar to the findings of Milne and Mitrovica (2008), who investigated the impact of the choice of Earth model on the non-barystatic signal, we find that uncertainty associated with poor knowledge of global ice history can reach up to 15/6 m at 21/6 ka BP, indicating that ice history uncertainty is an essential factor to consider when mapping global BSL history.

3.4. Future Development

In this study, we demonstrate that SCNNs can emulate RSL for a range of ice histories, assuming one specific Earth model. However, Earth rheology is a highly uncertain parameter that can result in hundreds of meters of RSL uncertainty in near-field regions and tens of meters in far-field regions. Therefore, an ideal GIA emulator should be able to sample ice history and Earth rheological properties simultaneously. One way to achieve this would be to incorporate Earth rheological parameters into the input data or a particular layer of the neural network. This would enable solid Earth rheology information to be considered when performing the convolution operations. While this is conceptually straightforward, it significantly complicates the computational task of constructing an emulator: considerably more training data would be required to fully sample the range of possibilities, and the relationship between model inputs and outputs would increase in complexity. Further investigation is required to develop an efficient and effective implementation of this concept, but as GEORGIA is an open-sourced model built upon a popular machine learning framework (PyTorch, Paszke et al., 2017), it is easily scalable for any further developments.

4. Conclusions

Using a graph-based SCNN, we document the first attempt to build a statistical GIA emulator (GEORGIA) that can approximate global RSL variation history based on a given deglacial ice history. GEORGIA predicts RSL history 100–1,000 times faster than a physics-based GIA model, with a MAE of 0.54 m. Due to its low computation expense, it is a suitable tool for performing large-ensemble investigations of ice history uncertainty. By providing example applications of GEORGIA—calculating the ice-sheet contribution to global BSL change and creating a BSL change map—we demonstrate that GEORGIA will be a useful tool for improving our understanding of global ice and sea-level variation histories.

Conflict of Interest

The authors declare no conflicts of interest relevant to this study.

Data Availability Statement

The spherical neural networks used in this study were built by the *DeepSphere* package which can be found at <https://github.com/deepsphere/deepsphere-pytorch>. GEORGIA, GEORGIA ensemble, along with the codes for creating example applications and visualization, are available at https://github.com/yc-lin-geo/Georgia_GIA, and Zenodo database with identifier <https://zenodo.org/record/8216017>.

References

- Abe-Ouchi, A., Saito, F., Kawamura, K., Raymo, M. E., Okuno, J., Takahashi, K., & Blatter, H. (2013). Insolation-driven 100,000-year glacial cycles and hysteresis of ice-sheet volume. *Nature*, *500*(7461), 190–193. <https://doi.org/10.1038/nature12374>
- Albrecht, T., Winkelmann, R., & Levermann, A. (2020). Glacial-cycle simulations of the Antarctic Ice Sheet with the Parallel Ice Sheet Model (PISM)—Part 2: Parameter ensemble analysis. *The Cryosphere*, *14*(2), 633–656. <https://doi.org/10.5194/tc-14-633-2020>

Acknowledgments

We thank Roger Creel and Lev Tarasov for their constructive reviews, which helped to significantly improve this paper. The authors thank Glenn A. Milne for providing the code used to perform the GIA modeling, Parviz Ajourlou and Ryan Love for useful discussion, Kurt Lambeck and Anthony Purcell for sharing the ANU ice model. Y.L. was supported by a China Scholarship Council—Durham University joint scholarship. A.P.V acknowledges support from the Australian Research Council under Grant DP200100053. This work made use of the facilities of the N8 Centre of Excellence in Computationally Intensive Research (N8 CIR) provided and funded by the N8 research partnership and EPSRC (Grant EP/T022167/1). The Centre is co-ordinated by the Universities of Durham, Manchester and York. The authors acknowledge the collaborative research opportunities created by PALSEA, a working group of the International Union for Quaternary Sciences (INQUA) and Past Global Changes (PAGES), which in turn received support from the Swiss Academy of Sciences and the Chinese Academy of Sciences.

- Argus, D. F., Peltier, W., Drummond, R., & Moore, A. W. (2014). The Antarctica component of postglacial rebound model ICE-6G_C (VM5a) based on GPS positioning, exposure age dating of ice thicknesses, and relative sea level histories. *Geophysical Journal International*, 198(1), 537–563. <https://doi.org/10.1093/gji/ggu140>
- Bassett, S. E., Milne, G. A., Mitrovica, J. X., & Clark, P. U. (2005). Ice sheet and solid earth influences on far-field sea-level histories. *Science*, 309(5736), 925–928. <https://doi.org/10.1126/science.1111575>
- Berdahl, M., Leguy, G., Lipscomb, W. H., & Urban, N. M. (2021). Statistical emulation of a perturbed basal melt ensemble of an ice sheet model to better quantify Antarctic sea level rise uncertainties. *The Cryosphere*, 15(6), 2683–2699. <https://doi.org/10.5194/tc-15-2683-2021>
- Briggs, R. D., Pollard, D., & Tarasov, L. (2014). A data-constrained large ensemble analysis of Antarctic evolution since the Eemian. *Quaternary Science Reviews*, 103, 91–115. <https://doi.org/10.1016/j.quascirev.2014.09.003>
- Brunet, D., Vrscay, E. R., & Wang, Z. (2011). On the mathematical properties of the structural similarity index. *IEEE Transactions on Image Processing*, 21(4), 1488–1499. <https://doi.org/10.1109/tip.2011.2173206>
- Caron, L., Ivins, E., Larour, E., Adhikari, S., Nilsson, J., & Blewitt, G. (2018). GIA model statistics for GRACE hydrology, cryosphere, and ocean science. *Geophysical Research Letters*, 45(5), 2203–2212. <https://doi.org/10.1002/2017gl076644>
- Clark, C. D., Chiverrell, R. C., Fabel, D., Hindmarsh, R. C., Ó Cofaigh, C., & Scourse, J. D. (2021). Timing, pace and controls on ice sheet retreat: An introduction to the BRITICE-CHRONO transect reconstructions of the British–Irish Ice Sheet. *Journal of Quaternary Science*, 36(5), 673–680. <https://doi.org/10.1002/jqs.3326>
- Dalton, A. S., Margold, M., Stokes, C. R., Tarasov, L., Dyke, A. S., Adams, R. S., et al. (2020). An updated radiocarbon-based ice margin chronology for the last deglaciation of the North American ice sheet complex. *Quaternary Science Reviews*, 234, 106223. <https://doi.org/10.1016/j.quascirev.2020.106223>
- Defferrard, M., Milani, M., Gusset, F., & Perraudin, N. (2020). DeepSphere: A graph-based spherical CNN. arXiv preprint arXiv:2012.15000.
- Defferrard, M., Perraudin, N., Kacprzak, T., & Sgier, R. (2019). DeepSphere: Towards an equivariant graph-based spherical CNN. arXiv preprint arXiv:1904.05146.
- Deschamps, P., Durand, N., Bard, E., Hamelin, B., Camoin, G., Thomas, A. L., et al. (2012). Ice-sheet collapse and sea-level rise at the Bølling warming 14,600 years ago. *Nature*, 483(7391), 559–564. <https://doi.org/10.1038/nature10902>
- Dziewonski, A. M., & Anderson, D. L. (1981). Preliminary reference Earth model. *Physics of the Earth and Planetary Interiors*, 25(4), 297–356. [https://doi.org/10.1016/0031-9201\(81\)90046-7](https://doi.org/10.1016/0031-9201(81)90046-7)
- Edwards, T. L., Nowicki, S., Marzeion, B., Hock, R., Goelzer, H., Seroussi, H., et al. (2021). Projected land ice contributions to twenty-first-century sea level rise. *Nature*, 593(7857), 74–82. <https://doi.org/10.1038/s41586-021-03302-y>
- Farrell, W., & Clark, J. A. (1976). On postglacial sea level. *Geophysical Journal International*, 46(3), 647–667. <https://doi.org/10.1111/j.1365-246x.1976.tb01252.x>
- Frederikse, T., Landerer, F., Caron, L., Adhikari, S., Parkes, D., Humphrey, V. W., et al. (2020). The causes of sea-level rise since 1900. *Nature*, 584(7821), 393–397. <https://doi.org/10.1038/s41586-020-2591-3>
- Gomez, N., Weber, M. E., Clark, P. U., Mitrovica, J. X., & Han, H. K. (2020). Antarctic ice dynamics amplified by Northern Hemisphere sea-level forcing. *Nature*, 587(7835), 600–604. <https://doi.org/10.1038/s41586-020-2916-2>
- Goodfellow, I., Bengio, Y., & Courville, A. (2016). *Deep learning*. MIT Press.
- Gorski, K. M., Hivon, E., Banday, A. J., Wandelt, B. D., Hansen, F. K., Reinecke, M., & Bartelmann, M. (2005). Healpix: A framework for high-resolution discretization and fast analysis of data distributed on the sphere. *The Astrophysical Journal*, 622(2), 759–771. <https://doi.org/10.1086/427976>
- Gowan, E., Tregoning, P., Purcell, A., Lea, J., Fransner, O. J., Noormets, R., et al. (2016). ICESHEET 1.0: A program to produce paleo-ice sheet reconstructions with minimal assumptions.
- Gowan, E. J., Zhang, X., Khosravi, S., Rovere, A., Stocchi, P., Hughes, A. L., et al. (2021). A new global ice sheet reconstruction for the past 80 000 years. *Nature Communications*, 12(1), 1–9. <https://doi.org/10.1038/s41467-021-21469-w>
- Han, H. K., Gomez, N., Pollard, D., & DeConto, R. (2021). Modeling northern hemispheric ice sheet dynamics, sea level change, and solid earth deformation through the last glacial cycle. *Journal of Geophysical Research: Earth Surface*, 126(4), e2020JF006040. <https://doi.org/10.1029/2020jf006040>
- Hay, C. C., Morrow, E., Kopp, R. E., & Mitrovica, J. X. (2015). Probabilistic reanalysis of twentieth-century sea-level rise. *Nature*, 517(7535), 481–484. <https://doi.org/10.1038/nature14093>
- Hibbert, F., Williams, F., Fallon, S., & Rohling, E. (2018). A database of biological and geomorphological sea-level markers from the Last Glacial Maximum to present. *Scientific Data*, 5(1), 180088. <https://doi.org/10.1038/sdata.2018.88>
- Hore, A., & Ziou, D. (2010). Image quality metrics: PSNR vs. SSIM. In *2010 20th international conference on pattern recognition* (pp. 2366–2369). IEEE.
- Huynh-Thu, Q., & Ghanbari, M. (2008). Scope of validity of PSNR in image/video quality assessment. *Electronics Letters*, 44(13), 800–801. <https://doi.org/10.1049/el:20080522>
- Kendall, R. A., Mitrovica, J. X., & Milne, G. A. (2005). On post-glacial sea level—II. Numerical formulation and comparative results on spherically symmetric models. *Geophysical Journal International*, 161(3), 679–706. <https://doi.org/10.1111/j.1365-246x.2005.02553.x>
- Korhonen, J., & You, J. (2012). Peak signal-to-noise ratio revisited: Is simple beautiful? In *2012 fourth international workshop on quality of multimedia experience* (pp. 37–38). IEEE.
- Lai, C.-Y., Kingslake, J., Wearing, M. G., Chen, P.-H. C., Gentile, P., Li, H., et al. (2020). Vulnerability of Antarctica's ice shelves to meltwater-driven fracture. *Nature*, 584(7822), 574–578. <https://doi.org/10.1038/s41586-020-2627-8>
- Lakshminarayanan, B., Pritzel, A., & Blundell, C. (2017). Simple and scalable predictive uncertainty estimation using deep ensembles. *Advances in Neural Information Processing Systems*, 30.
- Lambeck, K., Rouby, H., Purcell, A., Sun, Y., & Sambridge, M. (2014). Sea level and global ice volumes from the Last Glacial Maximum to the Holocene. *Proceedings of the National Academy of Sciences of the United States of America*, 111(43), 15296–15303. <https://doi.org/10.1073/pnas.1411762111>
- Lin, Y., Hibbert, F. D., Whitehouse, P. L., Woodroffe, S. A., Purcell, A., Shennan, I., & Bradley, S. L. (2021). A reconciled solution of Meltwater Pulse 1A sources using sea-level fingerprinting. *Nature Communications*, 12(1), 1–11. <https://doi.org/10.1038/s41467-021-21990-y>
- Lin, Y., Whitehouse, P. L., Hibbert, F. D., Woodroffe, S. A., Hineostroza, G., & Webster, J. M. (2023). Relative sea level response to mixed carbonate-siliciclastic sediment loading along the Great Barrier Reef margin. *Earth and Planetary Science Letters*, 607, 118066. <https://doi.org/10.1016/j.epsl.2023.118066>
- Love, R., Milne, G. A., Tarasov, L., Engelhart, S. E., Hijma, M. P., Latychev, K., et al. (2016). The contribution of glacial isostatic adjustment to projections of sea-level change along the Atlantic and gulf coasts of North America. *Earth's Future*, 4(10), 440–464. <https://doi.org/10.1002/2016ef000363>

- Milne, G. A., & Mitrovica, J. X. (1996). Postglacial sea-level change on a rotating Earth: First results from a gravitationally self-consistent sea-level equation. *Geophysical Journal International*, 126(3), F13–F20. <https://doi.org/10.1111/j.1365-246x.1996.tb04691.x>
- Milne, G. A., & Mitrovica, J. X. (2008). Searching for eustasy in deglacial sea-level histories. *Quaternary Science Reviews*, 27(25–26), 2292–2302. <https://doi.org/10.1016/j.quascirev.2008.08.018>
- Mitrovica, J., & Milne, G. (2002). On the origin of late Holocene sea-level highstands within equatorial ocean basins. *Quaternary Science Reviews*, 21(20–22), 2179–2190. [https://doi.org/10.1016/s0277-3791\(02\)00080-x](https://doi.org/10.1016/s0277-3791(02)00080-x)
- Mitrovica, J. X., Wahr, J., Matsuyama, I., & Paulson, A. (2005). The rotational stability of an ice-age Earth. *Geophysical Journal International*, 161(2), 491–506. <https://doi.org/10.1111/j.1365-246x.2005.02609.x>
- Paszke, A., Gross, S., Chintala, S., Chanan, G., Yang, E., DeVito, Z., et al. (2017). Automatic differentiation in pytorch.
- Patton, H., Hubbard, A., Andreassen, K., Auriac, A., Whitehouse, P. L., Stroeven, A. P., et al. (2017). Deglaciation of the Eurasian ice sheet complex. *Quaternary Science Reviews*, 169, 148–172. <https://doi.org/10.1016/j.quascirev.2017.05.019>
- Patton, H., Hubbard, A., Andreassen, K., Winsborrow, M., & Stroeven, A. P. (2016). The build-up, configuration, and dynamical sensitivity of the Eurasian ice-sheet complex to Late Weichselian climatic and oceanic forcing. *Quaternary Science Reviews*, 153, 97–121. <https://doi.org/10.1016/j.quascirev.2016.10.009>
- Peltier, W., Argus, D., & Drummond, R. (2015). Space geodesy constrains ice age terminal deglaciation: The global ICE-6G_C (VM5a) model. *Journal of Geophysical Research: Solid Earth*, 120(1), 450–487. <https://doi.org/10.1002/2014jb011176>
- Peltier, W. R. (2004). Global glacial isostasy and the surface of the ice-age earth: The ICE-5G (VM2) model and grace. *Annual Review of Earth and Planetary Sciences*, 32(1), 111–149. <https://doi.org/10.1146/annurev.earth.32.082503.144359>
- Perraudin, N., Defferrard, M., Kacprzak, T., & Sgier, R. (2019). DeepSphere: Efficient spherical convolutional neural network with healpix sampling for cosmological applications. *Astronomy and Computing*, 27, 130–146. <https://doi.org/10.1016/j.ascom.2019.03.004>
- Pittard, M. L., Whitehouse, P. L., Bentley, M. J., & Small, D. (2022). An ensemble of Antarctic deglacial simulations constrained by geological observations. *Quaternary Science Reviews*, 298, 107800. <https://doi.org/10.1016/j.quascirev.2022.107800>
- Reichstein, M., Camps-Valls, G., Stevens, B., Jung, M., Denzler, J., Carvalhais, N., & Prabhat (2019). Deep learning and process understanding for data-driven Earth system science. *Nature*, 566(7743), 195–204. <https://doi.org/10.1038/s41586-019-0912-1>
- Ronneberger, O., Fischer, P., & Brox, T. (2015). U-Net: Convolutional networks for biomedical image segmentation. In *International conference on medical image computing and computer-assisted intervention* (pp. 234–241). Springer.
- Roy, K., & Peltier, W. (2018). Relative sea level in the Western Mediterranean basin: A regional test of the ICE-7G_NA (VM7) model and a constraint on late Holocene Antarctic deglaciation. *Quaternary Science Reviews*, 183, 76–87. <https://doi.org/10.1016/j.quascirev.2017.12.021>
- Sacks, J., Welch, W. J., Mitchell, T. J., & Wynn, H. P. (1989). Design and analysis of computer experiments. *Statistical Science*, 4(4), 409–423. <https://doi.org/10.1214/ss/1177012413>
- Sefton, J. (2020). Evaluating mangrove proxies for quantitative relative sea-level reconstructions PhD thesis. Durham University.
- Simms, A. R., Lisiecki, L., Gebbie, G., Whitehouse, P. L., & Clark, J. F. (2019). Balancing the last glacial maximum (LGM) sea-level budget. *Quaternary Science Reviews*, 205, 143–153. <https://doi.org/10.1016/j.quascirev.2018.12.018>
- Tarasov, L., Dyke, A. S., Neal, R. M., & Peltier, W. R. (2012). A data-calibrated distribution of deglacial chronologies for the North American ice complex from glaciological modeling. *Earth and Planetary Science Letters*, 315, 30–40. <https://doi.org/10.1016/j.epsl.2011.09.010>
- Tarasov, L., Hughes, A., Gyllencreutz, R., Lohne, O. S., Mangerud, J., & Svendsen, J.-I. (2014). The global GLAC-1c deglaciation chronology, meltwater pulse 1-a, and a question of missing ice. In *IGS symposium: Contribution of glaciers and ice sheets to sea-level change* (pp. 26–30).
- Tarasov, L., & Peltier, W. (2005). Arctic freshwater forcing of the Younger Dryas cold reversal. *Nature*, 435(7042), 662–665. <https://doi.org/10.1038/nature03617>
- Tarasov, L., & Peltier, W. R. (2003). Greenland glacial history, borehole constraints, and Eemian extent. *Journal of Geophysical Research*, 108(B3), 2143. <https://doi.org/10.1029/2001jb001731>
- Waelbroeck, C., Labeyrie, L., Michel, E., Duplessy, J.-C., Mcmanus, J. F., Lambeck, K., et al. (2002). Sea-level and deep water temperature changes derived from benthic foraminifera isotopic records. *Quaternary Science Reviews*, 21(1–3), 295–305. [https://doi.org/10.1016/s0277-3791\(01\)00101-9](https://doi.org/10.1016/s0277-3791(01)00101-9)
- Wang, Z., & Bovik, A. C. (2009). Mean squared error: Love it or leave it? A new look at signal fidelity measures. *IEEE Signal Processing Magazine*, 26(1), 98–117. <https://doi.org/10.1109/msp.2008.930649>
- Webster, J. M., Braga, J. C., Humblet, M., Potts, D. C., Iryu, Y., Yokoyama, Y., et al. (2018). Response of the Great Barrier Reef to sea-level and environmental changes over the past 30,000 years. *Nature Geoscience*, 11(6), 426–432. <https://doi.org/10.1038/s41561-018-0127-3>
- Whitehouse, P. L. (2018). Glacial isostatic adjustment modelling: Historical perspectives, recent advances, and future directions. *Earth Surface Dynamics*, 6(2), 401–429. <https://doi.org/10.5194/esurf-6-401-2018>
- Whitehouse, P. L., Bentley, M. J., & Le Brocq, A. M. (2012). A deglacial model for Antarctica: Geological constraints and glaciological modelling as a basis for a new model of Antarctic glacial isostatic adjustment. *Quaternary Science Reviews*, 32, 1–24. <https://doi.org/10.1016/j.quascirev.2011.11.016>
- Whitehouse, P. L., Bentley, M. J., Milne, G. A., King, M. A., & Thomas, I. D. (2012). A new glacial isostatic adjustment model for Antarctica: Calibrated and tested using observations of relative sea-level change and present-day uplift rates. *Geophysical Journal International*, 190(3), 1464–1482. <https://doi.org/10.1111/j.1365-246x.2012.05557.x>
- Woodroffe, S. A., Long, A. J., Milne, G. A., Bryant, C. L., & Thomas, A. L. (2015). New constraints on late Holocene eustatic sea-level changes from Mahé, Seychelles. *Quaternary Science Reviews*, 115, 1–16. <https://doi.org/10.1016/j.quascirev.2015.02.011>
- Xu, K., Zhang, M., Li, J., Du, S. S., Kawarabayashi, K.-I., & Jegelka, S. (2020). How neural networks extrapolate: From feedforward to graph neural networks. arXiv preprint arXiv:2009.11848.
- Yao, W., Zeng, Z., Lian, C., & Tang, H. (2018). Pixel-wise regression using U-Net and its application on pansharpening. *Neurocomputing*, 312, 364–371. <https://doi.org/10.1016/j.neucom.2018.05.103>